JTTEE5 6:345-352

Mathematical Modeling of the Gas and Powder Flow in HVOF Systems

H.H. Tawfik and F. Zimmerman

A mathematical model was developed to describe the gas dynamics and heat-transfer mechanism in the gas/particle flow of high-velocity oxyfuel (HVOF) systems. A numerical solution was carried out using a PC-based computer program. One-dimensional predictions of the temperature and velocity profiles of gas and particles along the axis of flow were obtained to conduct cost-effective parametric studies and quality optimization of thermal spray coatings produced by HVOF systems. The numerical computer model allows for the variation of the HVOF system parameters, such as air/fuel ratio and flow rates, cooling water inlet temperature and flow rate, barrel length, standoff distance, particle size, and gun geometry.

Because of the negligible volume of the powder relative to the gas, the gaseous phase was modeled as continuous nonadiabatic, and friction flow with variable specific heats and changing cross-sectional areas of flow. The generalized continuity, momentum, and energy equations with the influence parameters were used to model the gaseous flow regime and predict its thermodynamic properties. Empirical formulas for the mean axial decay of both velocity and temperature in the supersonic jet plume region were generated from published measurements of these parameters using laser Doppler velocimeter and Rayleigh scattering techniques, respectively. The particle drag and heat-transfer coefficients were calculated by empirical formulas in terms of Reynolds, Nusselt, and Prandtl numbers to evaluate both the momentum and heat transferred between the combustion gases and the powder particles. The model predictions showed good agreement with the particle and gas temperature and velocity measurements that are available in the literature.

Keywords HVOF, model, optimization, parameters, quality

1. Introduction

Thermally sprayed coatings enhance materials properties and provide surface protection against their working environments in a number of industrial applications. Recently, hexavalent chromium associated with hard chromium plating was classified as a human carcinogen and environmental pollutant (Ref 1). The aerospace industry has traditionally used hard chrome plating as a corrosion protection material. Accordingly, the National Aeronautics and Space Administration (NASA) is developing thermal spray coatings to replace the hard chrome plating that is currently being used on the space shuttle main engine. These coatings are made of tungsten carbide and cobalt, chromium oxide, and FerroTic (iron-base material with titanium carbide) (Ref 1) to provide protection against wear, corrosion, and hydrogen embrittlement of the low-pressure liquid-hydrogen-carrying ducts on the shuttle main engine. One of these sections is the low-pressure fuel turbo pump (LPFTP) discharge duct used on the shuttle main engine. The duct carries liquid hydrogen fuel at a temperature of –253 °C (–423 °F) to the high-pressure fuel turbo pump (Ref 2).

In addition to its extensive use in generating protective coatings, thermal spray has been used in the manufacture of near-net-shape parts with customized material and engineered properties. In these applications, thermal spray is used to build up material(s) to form the required part geometry. Moreover, thermal spray is used for the repair of worn or mismachined mechanical parts (Ref 3).

Thermal spray coatings are formed from the flattened consolidation and solidification of molten powder particles; thus, the properties of these coatings are highly dependent on the spraying process itself. Accordingly, the microstructure, porosity, hardness, and bonding characteristics of the coatings are mainly controlled by the temperature and the velocity of molten particles (Ref 4).

High-velocity oxyfuel (HVOF) processes have proved successful for spray materials with melting points below 3000 K, since it shows economic advantages when compared to other coating processes that produce similar-quality coatings (Ref 5, 6). In such systems that produce high-velocity particles, the oxide content of the coatings did not correlate to the particle temperature or the excess oxygen in the lean fuel conditions, but it is related to high substrate temperatures (Ref 7). It is believed that the primary mechanism for the formation of oxide inclusions occurs after a particle splat, when the hot coating is exposed to the oxygen contained in the relatively low-velocity boundary layer. The exposure times of a given splat to the boundary layer are on the order of seconds, a factor of 10^3 longer than during particle flight (Ref 8).

The application of simulation techniques to thermal spray processes has grown steadily over the years. Once a model of the process is established and validated, system parameters become evident. The obtained fundamental understanding of the optimization process can be accomplished with a numerical computer model (Ref 6).

H.H. Tawfik, Manufacturing and Mechanical Research, State University of New York at Farmingdale, Farmingdale, NY, USA; and **F. Zimmerman,** Metals Processes Branch, Materials & Processes Laboratory, NASA Marshall Space Flight Center, Huntsville, AL, USA.

Accordingly, the objective of this investigation was to develop a computer model to simulate the thermal and gas dynamics of both gases and particles associated with the HVOF process to provide predictions of the particle velocities and temperatures. In the HVOF process, oxygen and atomized kerosene were injected coaxially into the combustion chamber, where they were mixed and ignited by a spark plug. The hot combustion gases were accelerated to supersonic conditions in a conversion diversion nozzle. At the exit of the nozzle, the powder was transversely injected with an argon or nitrogen carrier gas. The powder was heated and accelerated in the gun barrel and jet region by the hot gas, and most of the powder eventually was deposited on the substrate. The model was partially validated against data collected from Hobart Tafa using the JP-5000 system.

2. Mathematical Model

The model development was accomplished in four main stages as described in the following sections.

2.1 *First Stage: Modeling of the Gas Flow Inside the HVOF System with No Consideration of the Powder Flow (Ref 9)*

In most HVOF thermal spraying applications, the powder represents a small ratio of 5 to 8 wt% and negligible volume in relation to the combustion gases (Ref 10) that are considered the main continuous phase; therefore, the effect of the powder on the gas flow was ignored. The generalized flow equations with the influence parameters were used to model the gas flow in a HVOF. The temperature and mach number equations (Eq 1 and 2) were numerically integrated for a single-phase, nonadiabatic friction flow with variable specific heats (Ref 9). Thus:

$$\frac{dM^2}{M^2} = -2\frac{\left(1+\frac{k-1}{2}M^2\right)}{1-M^2}\frac{dA}{A} + \frac{1+kM^2}{1-M^2}\frac{dQ}{c_pT} + \frac{kM^2\left(1+\frac{k-1}{2}M^2\right)}{1-M^2}4f\frac{dx}{D} - \frac{dk}{k} \quad \text{(Eq 1)}$$

$$\frac{dT}{T} = \frac{(k-1)M^2}{(1-M^2)}\frac{dA}{A} + \frac{(1-kM^2)}{(1-M^2)}\frac{dQ}{c_pT} - \frac{k(k-1)M^4}{2(1-M^2)}4f\frac{dx}{D} \quad \text{(Eq 2)}$$

where A is the cross-sectional area of flow, f is the coefficient of friction, k is the ratio of specific heats, M is the mach number, Q is the net heat per unit mass of gas, T is absolute temperature, D is mean hydraulic diameter, X is the Cartesian coordinate, and c_p is the specific heat at constant pressure.

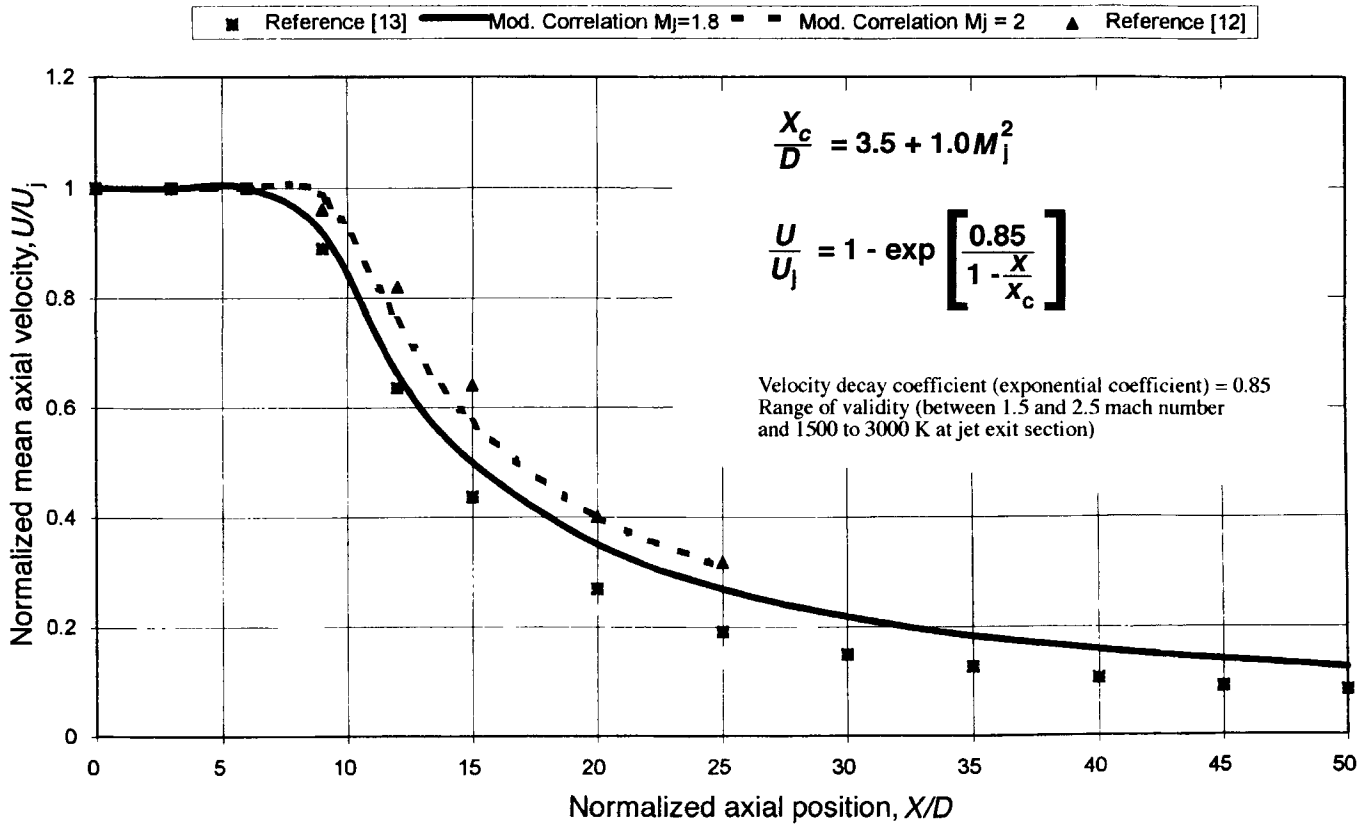

Fig. 1 Modified correlation for axial decay velocity in supersonic jet plumes

Equations 1 and 2 were solved by a numerical computer model, and predictions of the gas velocity and temperature were obtained (Ref 9) at all flow cross sections inside the thermal spray system. Due to the appearance of the term $(1 - M^2)$ in the denominator of Eq 1 and 2, the numerical model experienced singularity at the throat section of the convergent divergent nozzle. The model quickly recovered as the solution propagated downstream of the throat area. However, this singularity problem could be completely rectified by the application of a Taylor series expansion on these singularity-causing terms in the throat proximity zone.

2.2 *Second Stage: Empirical Correlation for the Mean Axial Velocity and Temperature Decay of a Free Supersonic Jet Plume*

Visual studies, such as Schlieren flow visualization, showed a "potential core" with an embedded shock-diamond structure that is formed in the supersonic zone due to the underexpanded nature of the jet (Ref 8). Further downstream, large turbulent eddies were generated by the large velocity and temperature gradients at the boundary layer between the jet and the ambient air. This mixing zone is further subjected to the effect of a large density difference between the hot jet core and the comparatively cold and slow ambient atmosphere. Particles smaller than 5 μm will fully track the turbulent motion of the fluid; however, much larger particles, such as typical HVOF metal spray powders, are generally unaffected by the eddies and remain in the relatively high-temperature, low-density, and least-motion-resistance zone near the jet centerline (Ref 8).

To better understand the noise generation mechanism in supersonic free jets, considerable investigation efforts have been devoted to the measurement of flow parameters and how these quantities vary with jet flow conditions (Ref 11). Earlier mean velocity measurements (Ref 11) using laser Doppler velocimeter and hot-wire anemometer techniques resulted in an empirical formula that gives the variation of the potential core length with the mach number for both heated and cooled jets:

$$\frac{X_c}{D} = 4.2 + 1.1 M_j^2 \qquad \text{(Eq 3)}$$

where X_c is potential core length, D is the exit jet diameter, and M_j is the exit jet mach number.

A general empirical correlation for the supersonic axial mean velocity decay with a range of validity between mach numbers 0.3 and 1.4 is (Ref 10):

$$\frac{U}{U_j} = 1 - \exp\left(\frac{1.35}{1 - \frac{X}{X_c}}\right) \qquad \text{(Eq 4)}$$

where U is the average jet velocity and U_j is the exit jet velocity.

In HVOF applications, the jet mean axial velocity and temperature ranges are between mach numbers 1.5 and 2.5 and 1500 and 3000 K, respectively. A study of heated jets indicated that the core length decreased as the jet temperature increased (Ref 12). Thus, Eq 3 and 4 were modified to expand their range of validity by correlating recent measurements of the mean axial decay velocity and temperature obtained from NASA/Langley (Ref 11) and the University of Toronto (Ref 13). Figures 1 and 2 show the mean velocity and temperature correlations in relation

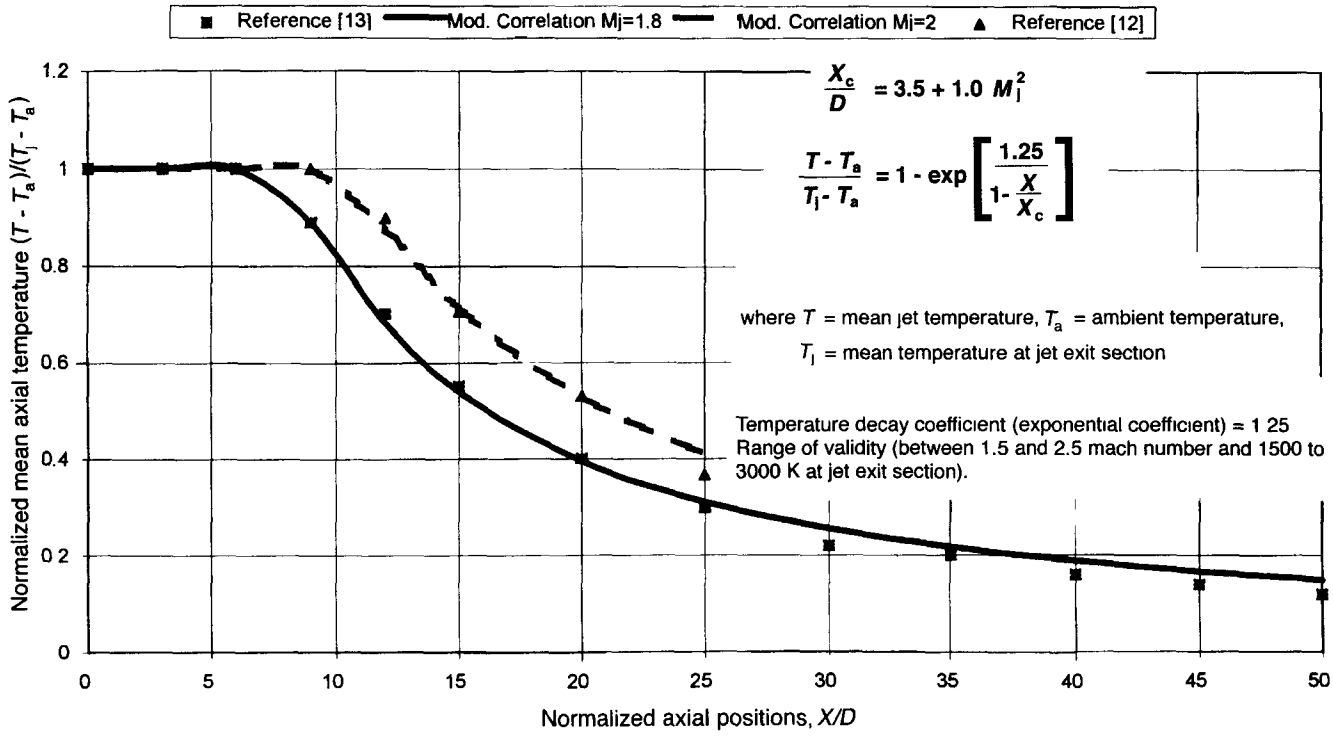

Fig. 2 Modified correlation for axial decay temperature for supersonic jet plumes

to the measured values. Comparison of these figures for free axisymmetrical jets indicated that the velocity decays faster than the temperature; that is, the momentum transfer between a jet and a still ambient is more pronounced than heat transfer between a heated jet and a cold surrounding environment. The decay coefficients are 0.85 and 1.25, as depicted in Fig. 1 and 2, respectively.

2.3 *Third Stage: Momentum Transfer Mechanism between Gas and Particle*

In a gas/solid or a gas/liquid flow, the momentum equations, for either solid or liquid particles, were solved in a Lagrangian frame of reference moving with the particles. The equation of motion for the particle is written as (Ref 14):

$$m_p \frac{dV_p}{dt} = \frac{1}{2} \rho_g A_p C_D (V_g - V_p)|V_g - V_p| - v_p \nabla p \qquad \text{(Eq 5)}$$

where m_p is the mass of the particle; V_p is the velocity vector of the particle; C_D is the drag coefficient; ρ_g, V_g, and p are the density, velocity, and pressure of the gas, respectively; A_p is the particle surface area; and v_p is the particle volume. The particle motion in two-phase flows depends on the gas properties and particle properties. Because of the relatively high surface tensions of liquid metals, all particles are assumed to maintain their near-spherical shape during the active heat-transfer periods in the barrel and the free plume. This equation of motion for a particle accounts for the acceleration/deceleration of the particle or droplet, due to the combined effects of drag from the gas flow and local pressure gradients in the gas. Because the gas flow pressure change is relatively small in the friction flow inside the gun barrel and the free jet plume, the gas pressure gradient effect on the particle motion is neglected in comparison to the drag force (Ref 9).

A literature survey in the area of two-phase flows reveals that a number of drag coefficient equations have been used to calculate particle motion in supersonic flows (Ref 15). Because the particles are injected into a supersonic flow, each particle will initially have a shock wave on the upstream side. As the particle accelerates and gains more speed downstream, the strength of the shock wave subsides and eventually diminishes. The drag induced on these particles in this supersonic flow is calculated with the following empirical correlation (Ref 15):

$$\frac{dV_p}{dt} = \frac{3}{4} C_D \left(\frac{\rho_g}{\rho_p}\right) \frac{(V_g - V_p)|V_g - V_p|}{d} \qquad \text{(Eq 6)}$$

The drag coefficient for the particle is based on the local Reynolds number of the particle and is evaluated as:

$$Re = \rho |V_g - V_p| \frac{d_p}{\mu} \qquad \text{(Eq 7)}$$

where μ is the molecular viscosity of the gas. The variation of the gas viscosity was evaluated from the graph and empirical formula shown in Fig. 3. The following correlations have been found to be valid for a wide range of Reynolds number (Ref 14):

$$C_D = \frac{24}{Re} \text{ for } Re < 1$$

$$C_D = \frac{24}{Re}(1 + 0.15 Re^{0.687}) \text{ for } 1 < Re < 10^3$$

$$C_D = 0.44 \text{ for } Re > 10^3 \qquad \text{(Eq 8)}$$

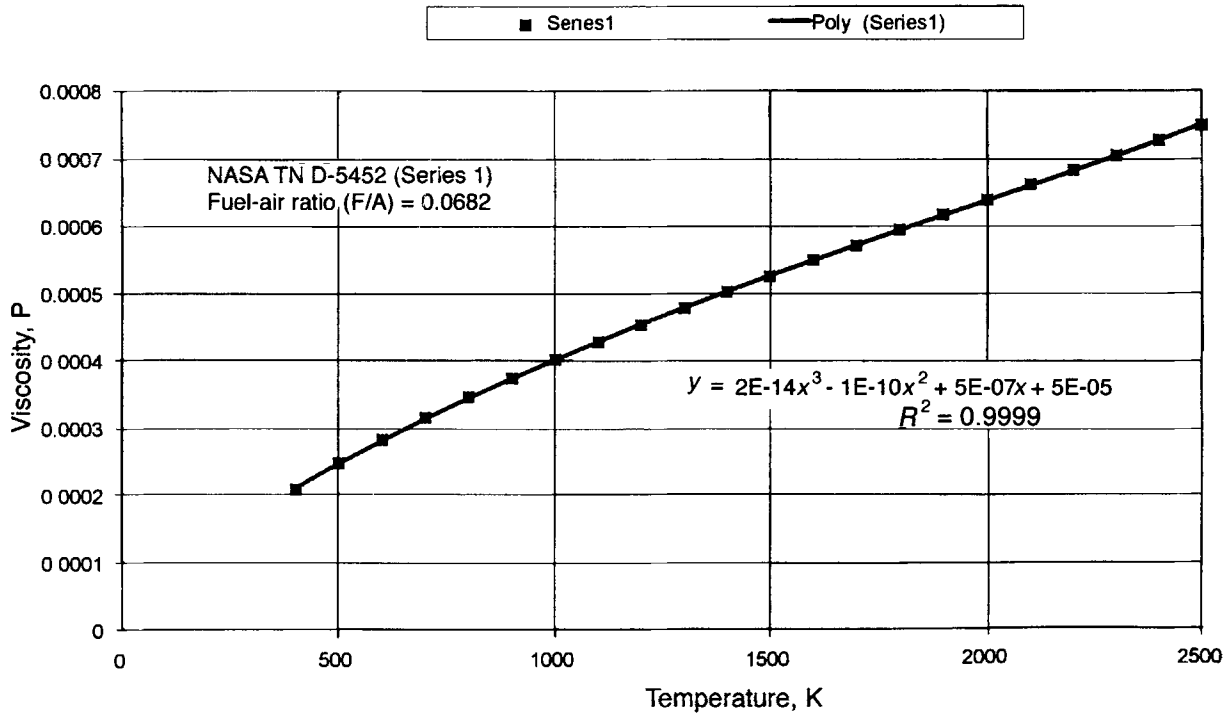

Fig. 3 Viscosity versus temperature for combustion gases of ASTM-A-1 burned in air at 3 atm

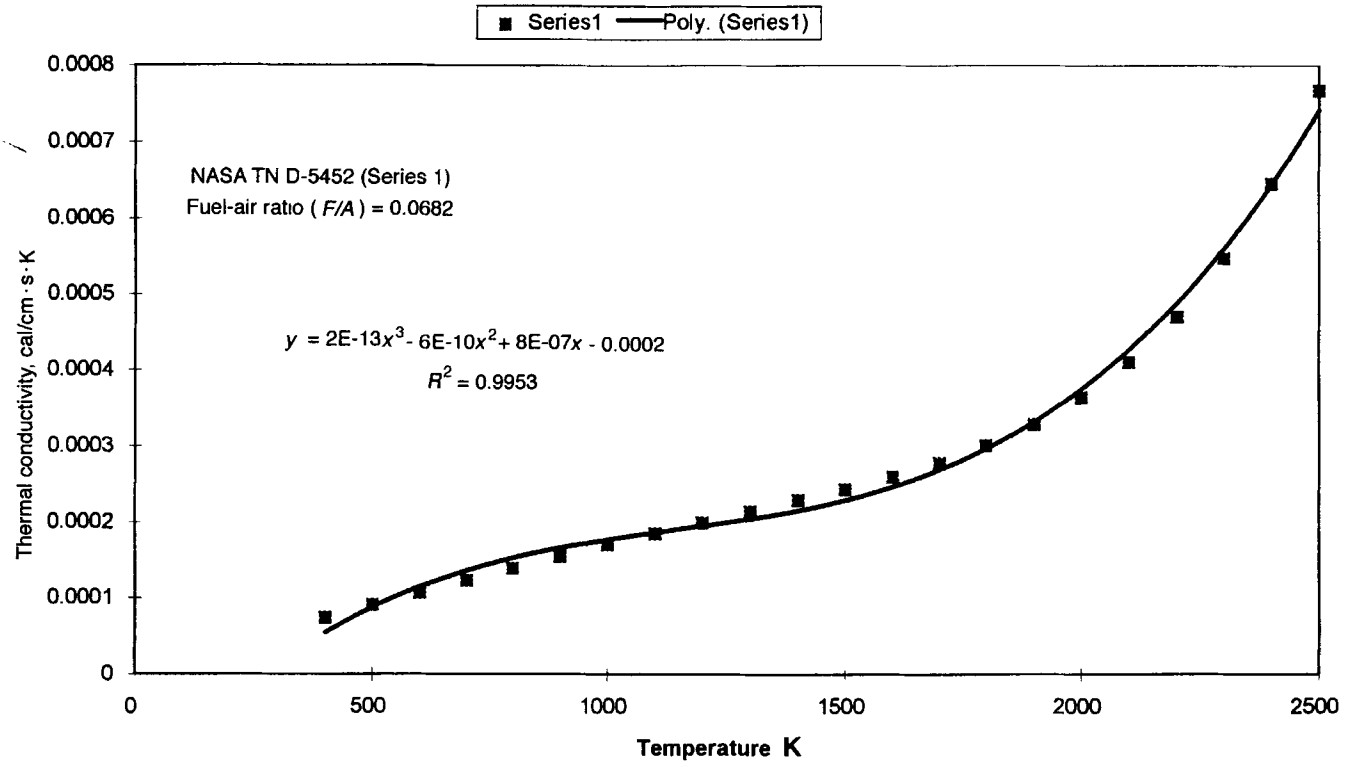

Fig. 4 Thermal conductivity versus temperature for combustion gases of ASTM-A-1 burned in air at 3 atm

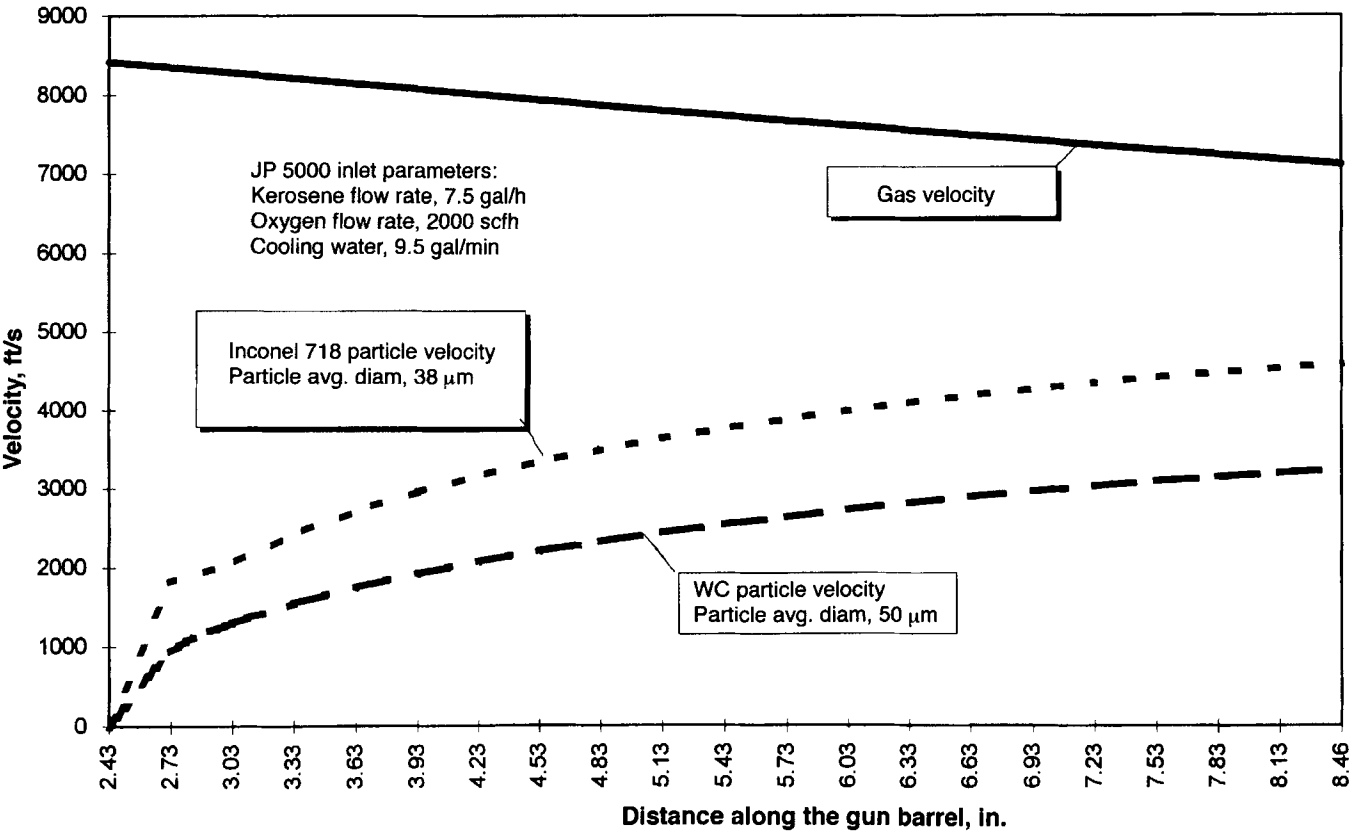

Fig. 5 Predicted gas and particle velocities inside the JP-5000 gun barrel

2.4 *Fourth Stage: Heat-Transfer Mechanism between the Gas and the Powder*

The coefficient of heat transfer (h) between the particle and the gas can be determined from the following Ranz-Marshall semiempirical equation:

$$Nu = \frac{hd_p}{k_g} = 2 + 0.6Re^{0.5}Pr^{0.3333}$$

$$Pr = \frac{c_{p_g}\mu_g}{k_g} \qquad \text{(Eq 9)}$$

where c_p is the specific heat of combustion gases, d_p is particle diameter, and k_g is the coefficient of gas thermal conductivity that was evaluated from a correlation as a function of temperature (Fig. 4). Considering that the particle maintained its spherical configuration throughout the process, and exhibited a homogeneous temperature distribution within the negligible particle volume in relation to the combustion gases, the temperature of the particle was calculated from Eq 10:

$$T_p = \frac{\Delta thT_g + \frac{1}{3}\rho_p R_p c_p T_{p_i}}{\Delta th + \frac{1}{3}\rho_p R_p c_p} \qquad \text{(Eq 10)}$$

3. Results and Discussion

The model predictions showed a sharp increase in both particle velocity and temperature when the powder was initially injected in the barrel (Fig. 5 and 6). The particle velocity reached almost half the gas velocity at the end of the barrel. Meanwhile, the particle temperature closely approached the gas temperature at the same location. This indicates that the heat-transfer mechanism between the gas and the particle is more efficient than the momentum-transfer mechanism. Also, the experimental measurements of normalized axial velocity and temperature of the supersonic heated plume, shown in Fig. 1 and 2, respectively, conveyed similar understanding since the decay exponent of the momentum transfer (0.85) was less than that of the heat transfer (1.25).

The model predictions of particle and gas velocities and temperatures in the jet plume (Fig. 7 and 8) showed that the gas maintained steady velocity and temperature over the potential core zone, which extends up to $X/D \approx 8$ to 10, due to the lack of significant ambient air entrainment in this zone. At the end of this zone, both the gas velocity and temperature experience a rapid decrease as they cross below the particle velocity and temperature curves shown in Fig. 7 and 8. This is attributed to large-scale eddies and turbulent entrainment of a comparatively much cooler and slower surrounding atmosphere in the mixing turbulent region of the jet generated by the shear boundary layer and the density difference between the jet and the environment. The overall effect is that the jet cooled, spread, and decelerated, as depicted in Fig. 7 and 8.

Figures 7 and 8 also show the velocity and temperature predictions of two different particles: tungsten carbide (WC) and Inconel 718. The predictions showed that the lighter Inconel 718 particle with a density almost half that of the WC particle gained and lost both heat and momentum faster than the WC particle, as clearly shown in Fig. 5 to 8.

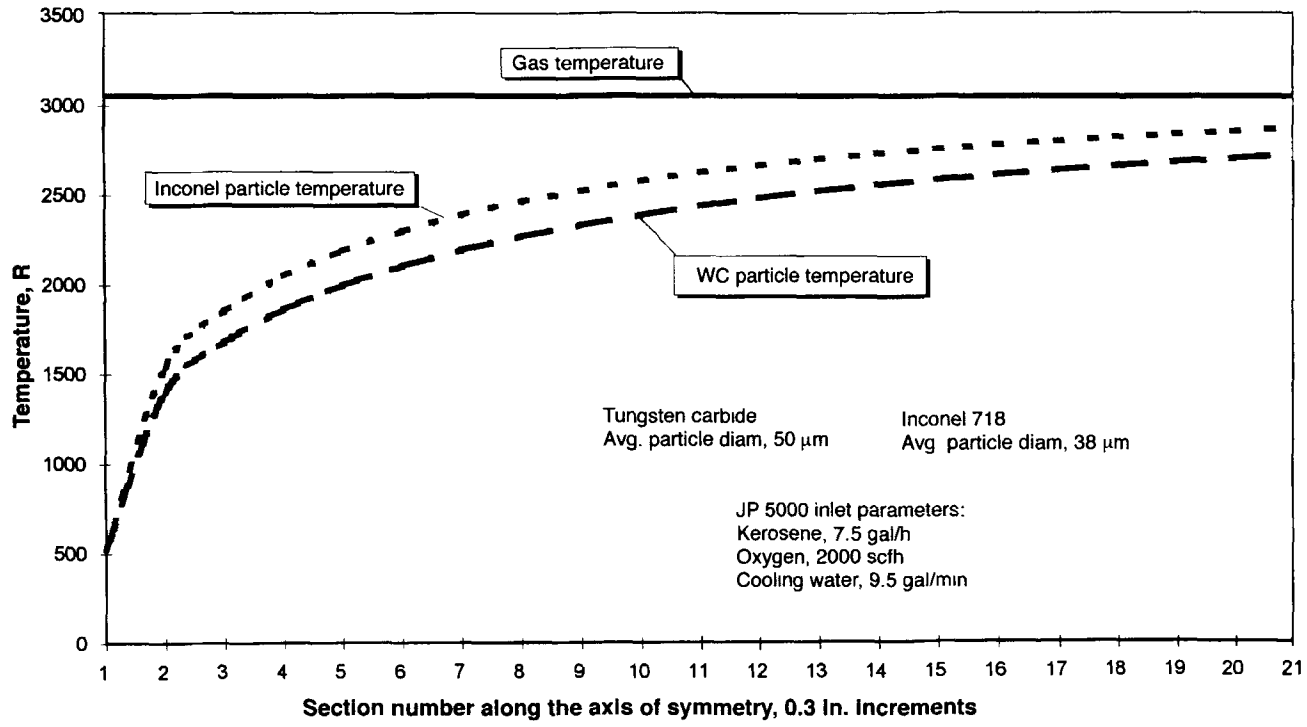

Fig. 6 Predicted gas and powder temperatures inside the JP-5000 gun barrel

The predicted values from the model showed good agreement with the experimental data published by the JP 5000 manufacturer. Accordingly, after complete validation this model could provide a powerful simulation and optimization tool for HVOF thermal spray systems and the coating quality produced by these systems.

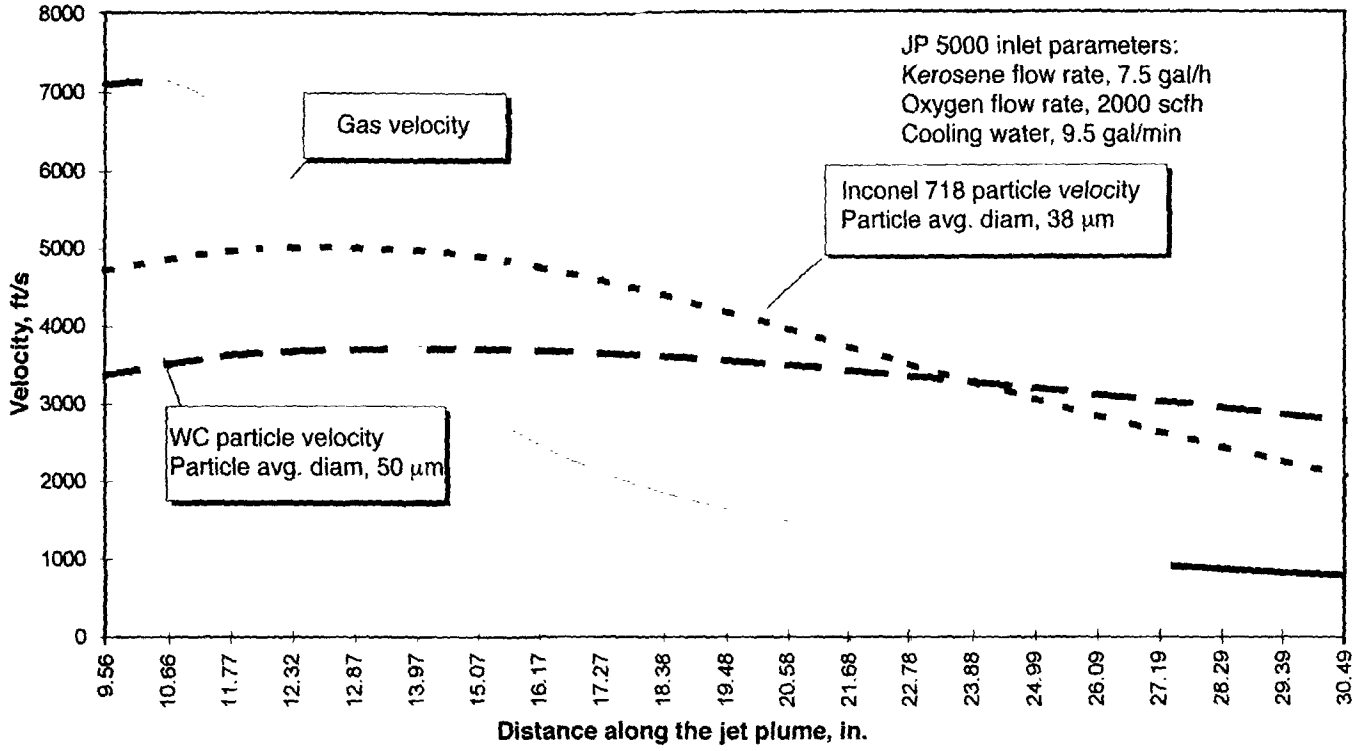

Fig. 7 Predicted gas and particle velocities in the free jet plume of an HVOF system

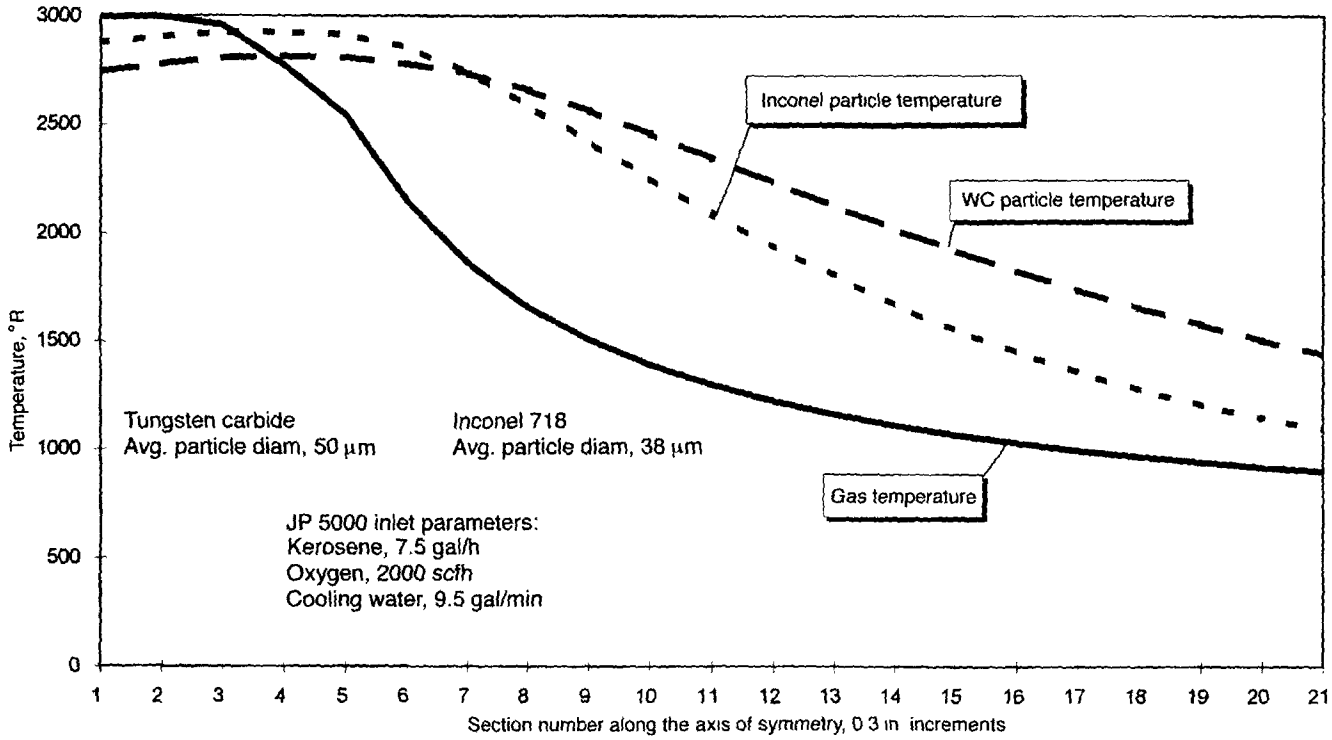

Fig. 8 Predicted gas and powder temperatures in the jet plume

4. Conclusions

- The model predictions showed the expected velocity and temperature trends for both the particles and the gas.
- The model was partially validated against measurements provided by the manufacturer.
- After validation, the model could be used for parametric study and optimization of HVOF systems.
- Singularity due to the $(1 - M^2)$ term briefly affected the model prediction around the throat area, but the model quickly recovered.

References

1. F. Zimmerman, NASA/Marshall Space Flight Center, private communication, 1995
2. R.L. Daniel, H.L. Sanders, and M.J. Mendrek, Replacement of Environmentally Hazardous Corrosion Protection Paints on the Space Shuttle Main Engine Using Wire Arc Sprayed Aluminum, *Thermal Spray Industrial Applications,* C.C. Berndt and S. Sampath, Ed., ASM International, 1994, p 93-98
3. D. Rome, Naval Surface Warfare Center, private communication, 1993
4. P. Siitonen, T. Konos, and P. Kettunen, Corrosion Properties of Stainless Steel Coatings Made by Different Methods of Thermal Spraying, *Thermal Spray Industrial Applications,* C.C. Berndt and S. Sampath, Ed., ASM International, 1994, p 105-110
5. R. Shah, K.-C. Wang, K. Parthasaathi, J. Jo, and E Onesto, Towards Manufacturing High-Quality Thermal Spray Coatings, *Thermal Spray Industrial Applications,* C.C. Berndt and S Sampath, Ed., ASM International, 1994, p 675-681
6. O. Knotek, E. Lugscheider, P. Jokiel, U. Schnaut, and A. Wiemers, Chromium Coatings by HVOF Thermal Spraying: Simulation and Practical Results, *Thermal Spray Industrial Applications,* C.C. Berndt and S. Sampath, Ed., ASM International, 1994, p 179-184
7. W.D. Swank, J.R. Fincke, D.C. Haggard, G. Irons, and R Bullock, HVOF Particle Flow Field Characteristics, *Thermal Spray Industrial Applications,* C.C. Berndt and S. Sampath, Ed., ASM International, 1994, p 319-324
8. C.M. Hackett and G S. Settles, Turbulent Mixing of the HVOF Thermal Spray and Coating Oxidation, *Thermal Spray Industrial Applications,* C.C. Berndt and S Sampath, Ed., ASM International, 1994, p 307-312
9. H. Tawfik and F. Zimmerman, "Quality Optimization of Thermally Sprayed Coatings Produced by HVOF Systems Using Mathematical Modeling," paper presented at NASA/ASEE Summer Faculty Fellowship Program, NASA Marshall Space Flight Center, 1994
10. TAFA, Inc., Technical Specifications JP 5000
11. J.C. Lau and P.J. Morris, Measurements in Subsonic and Supersonic Free Jets Using a Laser Velocimeter, *J. Fluid Mech.,* Vol 93, Part 1, 1979, p 1-27
12. N.T. Lagen and J.M. Seiner, "Evaluation of Water Cooled Supersonic Temperature and Pressure Probes for Application to 2000 °F Flows," NASA Technical Memorandum 102612
13. L.Y. Jiang and J.P. Sislian, "LDV Measurements of Mean Velocity Components and Turbulence Intensities in Supersonic High-Temperature Exhaust Plumes," AIAA-93-3067, American Institute of Aeronautics and Astronautics, 1993
14. W.L. Oberkampf and M. Talpallikar, Analysis of a High Velocity Oxygen-Fuel (HVOF) Thermal Spray Torch, Part 1: Numerical Formulation, *Thermal Spray Industrial Applications,* C.C. Berndt and S. Sampath, Ed., ASM International, 1994, p 381-386
15. M.L. Thorpe and H.J. Richter, A Pragmatic Analysis and Comparison of HVOF Processes, *J. Therm. Spray Technol.,* Vol 1 (No. 2), 1992, p 161-170